Journal of Molecular Graphics and Modelling 45 (2013) 45–49

Contents lists available at ScienceDirect

Journal of Molecular Graphics and Modelling

journal homepage: www.elsevier.com/locate/JMGM

Studies on argon collisions with smooth and rough tungsten surfaces

M.S. Ozhgibesov[a,*], T.S. Leu[a], C.H. Cheng[a], A.V. Utkin[b]

[a] Department of Aeronautics and Astronautics, National Cheng Kung University, Tainan 701, Taiwan, ROC
[b] Khristianovich Institute of Theoretical and Applied Mechanics, SBRAS, Novosibirsk, Russia

ARTICLE INFO

Article history:
Received 9 May 2013
Accepted 8 August 2013
Available online 20 August 2013

Keywords:
Molecular dynamics
Argon–tungsten collisions
OpenMP
CUDA

ABSTRACT

The aim of this work is to investigate argon scattering behaviors on the smooth and rough tungsten surfaces. Current work deals with numerical simulation of nanoscale heat transfer process accompanying with rarefied gas–solid substrate interactions using molecular dynamics (MD) method. Taking into account that this method is very time consuming, MD simulation using CUDA capable Graphic Cards is implemented. The results found that imperfection of the surface significantly influences on gas atom's momentum change upon collision. However, the energy exchange rate remains unchanged regardless to the surface roughness. This finding is in contrast with the results in extant literatures. We believed the results found in this paper are important for both numerical and theoretical analyses of rarefied gas flow in micro- and nano-systems where the choice of boundary conditions significantly influences flow.

1. Introduction

Improvements in micro/nano fabrication as well as reducing cost of the fabrication have increased the application areas of micro/nano systems [1]. This has motivated many engineers and researchers to develop micro-/nano-electro-mechanical-systems (MEMS or NEMS). Such micro/nano systems can be applied in a wide range of applications, such as in micro biochemical reaction chambers [2], heat exchangers [3] and gas detectors [4]. Most of these devices deal with the flow of gases or liquids. Recent technological advances allowed one to create MEMS/NEMS devices with characteristic size of several nanometers [1]. The design processes of such micro/nano devices are very expensive and complicated and involve both experimental and numerical studies of solid and fluid mechanics inside the device. It should be noted that micro/nano flow is characterized by a high degree of rarefaction. It means that assumption of classical continuum theory cannot be applied for analysis of micro/nano flow. Fortunately there is a numerical method, called molecular dynamics (MD) simulation method. It is based on the fundamental principles of mechanics and allows one to simulate processes on molecular level, i.e., the simulated system is considered as ensemble of molecules, rather than a continuous medium.

One of the most challenging parts of numerical simulations of a micro/nano flow is boundary conditions on the solid–liquid interface. The choice of model describing fluid–solid interactions influences on a flow significantly [5]. The energy/heat transfer and the scattering of rarefied gases from different surfaces were attracting attention of researchers for many years. One of the pioneers was Maxwell [6]. Maxwell proposed a relatively simple model where a gas impinging on a surface is scattered into two fractions, one that reflects specularly (without energy exchange) and another that accommodates completely and desorbs with an equilibrium distribution corresponding to temperature of the surface. Other studies of gas-surface interactions have focused on determining the thermal accommodation coefficients [7]. Weinberg and Merrill [8] determined angular distributions for gas atoms scattered by a single-crystal W(1 1 0) surface; and Janda et al. [9] measured velocity distributions for argon atoms scattering from a clean, polycrystalline tungsten surface. The experimental results of the second study allowed the researchers to relate the average kinetic energy of scattered argon atoms to the mean incident kinetic energy, as well as to the surface temperatures. In other representative study, Fan and Manson [10] discussed argon atoms scattering from a self-assembled monolayer on Ag(1 1 1). Furthermore, Gibson et al. [11] conducted a comprehensive study of Ar scattering from an ordered 1-decanethiol–Au(1 1 1) monolayer.

The aim of this work was to study the influence of surface's roughness on processes accompanying collisions of argon atoms with tungsten substrate. The method applied in the present paper can be simply expressed as the bombing of a tungsten surface with argon atoms, where further analysis of the scattered atoms' trajectories was conducted. Analysis of both angular distributions and distributions of velocities of scattered atoms were performed using mean values and root mean square deviations (RMSDs). This combination provided complete information regarding the scattering process.

* Corresponding author. Tel.: +886 989456028.
E-mail address: omiser@gmail.com (M.S. Ozhgibesov).

1093-3263/$ – see front matter © 2013 Elsevier Inc. All rights reserved.
http://dx.doi.org/10.1016/j.jmgm.2013.08.010

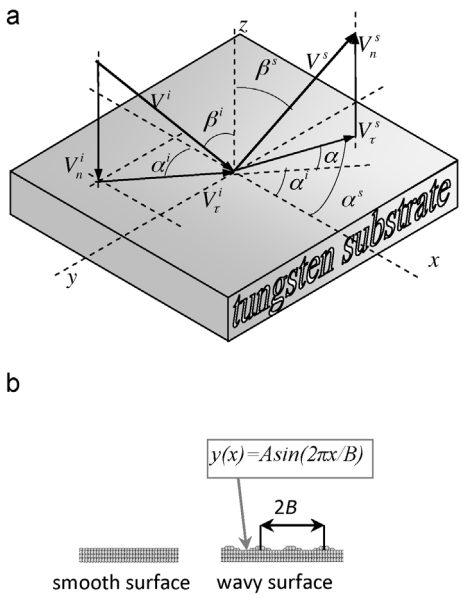

Fig. 1. (a) Coordinate system, where α^i and β^i – incident azimuthal and polar angles, respectively; α^S and β^S are scattered beam's azimuthal and polar angles, respectively; $\alpha = \alpha^S - \alpha^i$ – azimuthal angle change caused by the scattering of the beam; ${V_n}^i$ and ${V_\tau}^i$ – normal and tangential velocity components of the incident beam; ${V_n}^S$ and ${V_\tau}^S$ – normal and tangential velocity components of the scattered beam. (b) Side view of the smooth and wavy surfaces. *A* and *B* – amplitude and wavelength, respectively.

2. Methodology and computation

The model considered in this study included tungsten W(1 1 0) substrate with a temperature of T_{surf} and argon atoms with an impinging velocity vector magnitude V^i and velocity vector direction determined by the azimuthal (in horizontal plane) and polar (in vertical plane) angles α^i and β^i, respectively. The simulation procedure consisted of a tungsten substrate bombardment of argon atoms, after which the scattered atoms' parameters V^s, α^s and β^s were determined, as shown in Fig. 1a.

The substrate consisted of six atomic layers, and atoms that comprised the bottom layer were held fixed in their equilibrium lattice positions while the atoms in the other layers were permitted to move according to the appropriate classical equations of motion. In order to demonstrate the influence of a surface's irregularities on flow, two types of substrates with smooth (Fig. 1b – left picture) and wavy (Fig. 1b – right picture) surface are considered respectively. The initial velocities of the tungsten atoms were determined by the Maxwell distribution function corresponding to the desired temperature of the substrate. The simple velocity scaling method was used to maintain the temperature of the tungsten at a constant value.

Current research was performed numerically by using MD simulation method. All algorithms described in this study were utilized using code developed by the authors of this paper. It should be noted that MD simulations are very time consuming. However, the recent development of General Purpose Graphics Processing Units (GPGPU) and corresponding parallel programming languages provide a cost-effective solution for this issue. Compute Unified Device Architecture (CUDA) developed by NVIDIA has allowed one to use the power of Graphic Processing Units (GPU) for computations. The usage of GPUs for MD simulations is made further attractive due to their relatively low price, compact size and low power consumption compared to computer clusters. High-bandwidth memory and multithreading hardware implementation enable GPUs to outperform traditional CPU cores on data parallel workloads by factors ranging from ten to thirty times faster in most cases [12], and up to as much as one hundred times faster in a few ideal cases [13].

Table 1
Normalized time of execution of the MD program on different computational systems.

Number of atoms	CPU (intel i7-950)		GTX590 + GTX580
	Sequential 1 CPU	OpenMP 4 CPUs	CUDA + OpenMP
14,894	52.20	22.99	1.00
34,461	155.78	68.73	2.98
66,326	416.34	173.22	5.17
178,956	2258.29	919.00	19.67
265,721	4703.86	1849.05	33.89

In the current work, both OpenMP and CUDA technologies are applied. OpenMP allows us to share the job among CPU cores, while CUDA provides us with the advantage of using the GPU for computation. The combination of these technologies allows one to share the job among several GPUs by using the CPU to control the exchanges between the GPUs. Thus each separate CPU core governs a separate GPU. Two gaming graphic cards, NVIDIA GeForce GTX590 and GTX580 are used in the current research. It should be noted that the GTX590 consists of two graphic cards that can work separately. We have thus used 3 of the CPU's cores to control both the GTX590 and the GTX580 GPUs. The total number of GPU cores involved in our simulations is 1536. Detailed description of the parallel algorithm is presented in our previous studies [14,15]. Table 1 represents the normalized time of execution of the MD program on different computation systems. One can see that the parallel program run on CUDA GPUs outperforms the sequential one by about 130 times.

In order to evaluate the gas scattering effects, various collimated beams of argon atoms with intensity of 2×10^5 Pa are set up to impinge on the (1 1 0) face of a tungsten crystal. The interactions among tungsten atoms were taken as being sums of pairwise Morse potential:

$$\Phi_{W-W} = \begin{cases} D_W[e^{-2B_W(r-R_W)} - 2e^{-B_W(r-R_W)}], & 0 < r < 2.3R_W \\ 0, & r \geq 2.3R_W \end{cases} \quad (1)$$

where the potential's parameters [16] were: $D_W = 0.9906$ eV, $B_W = 14.116\ nm^{-1}$, $R_W = 0.3032$ nm.

To describe the interaction between both argon–tungsten and argon–argon atoms, Lennard–Jones potential functions are applied and depicted as following:

$$\Phi_{W-Ar} = \begin{cases} 4\varepsilon_{WAr}\left[\left(\frac{R_{WAr}}{r}\right)^{12} - \left(\frac{R_{WAr}}{r}\right)^{6}\right], & 0 < r < 2.5R_{WAr} \\ 0, & r \geq 2.5R_{WAr} \end{cases} \quad (2a)$$

$$\Phi_{Ar} = \begin{cases} 4\varepsilon_{Ar}\left[\left(\frac{R_{Ar}}{r}\right)^{12} - \left(\frac{R_{Ar}}{r}\right)^{6}\right], & 0 < r < 2.5R_{Ar} \\ 0, & r \geq 2.5R_{Ar} \end{cases}, \quad (2b)$$

where the parameters values used for the case of argon–tungsten and argon–argon, respectively, were: $\varepsilon_{WAr}/k_B = 25.17$ K, $R_{WAr} = 2.93$ Å and $\varepsilon_{Ar}/k_B = 119.18$ K, $R_{Ar} = 3.4$ Å.

The initial lateral position for the impinging atom was selected randomly on a plane 17 Å above the atoms of the uppermost solid layer. In order to model the scattering of a velocity-selected, collimated beam, the initial momentum of the incident atom was taken to be the same for each trajectory of a given set. The second order velocity Verlet integration scheme [16] with time step of $\Delta t = 10^{-16}$s (smaller than the characteristic time of atom interactions) was used for an integration of equations of motion. Scattered gas atoms that went beyond the force field of the tungsten atoms

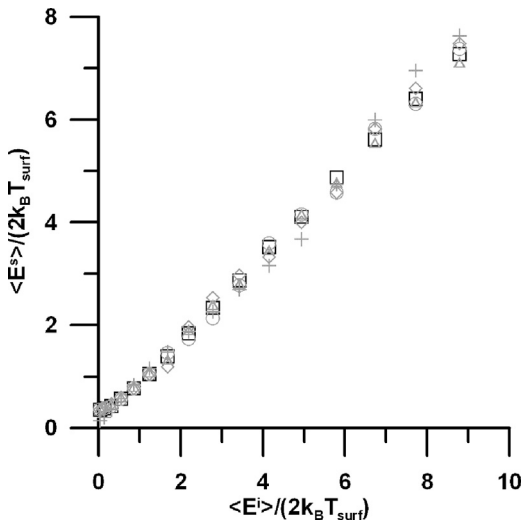

Fig. 2. Mean energy of scattered atoms versus energy of impinging atoms at $\beta^i = 45^\circ$. □, Surface Type A; ○, real surface Type B; Δ, surface Type C; ◊, surface Type D; +, surface Type E.

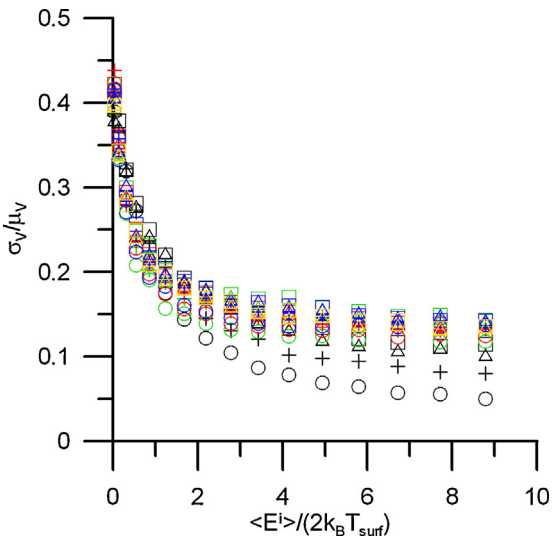

Fig. 3. Root mean square deviation of scattered atoms' velocities σ_V over mean velocity of scattered atoms μ_V versus kinetic energy of impinging atoms. □, $\beta^i = 10^\circ$; Δ, $\beta^i = 20^\circ$; +, $\beta^i = 40^\circ$; ○, $\beta^i = 60^\circ$. Black symbols correspond to a smooth surface. Green, red, blue and yellow symbols correspond to surfaces of Type B, C, D and E, respectively.

were excluded from the system (argon atoms did not pass through the tungsten substrate), and information on their velocity vectors were stored in a file. The exclusion of these scattered atoms reduces the time required for the calculation and prevents the randomization of motion of argon atoms as a consequence of their collision with each other. The computational process was continued until all the gas atoms were within the distance mentioned above.

3. Results and discussion

It is obvious that any analytical or numerical study is based on assumptions and simplified description of real processes. Consequently, results of such works must be compared with experimental results in order to prove the reasonability of simplifications. Fig. 2 shows the correlation of kinetic energy of impinging atoms (initial energy of the beam falling onto the surface) with the mean kinetic energy of the atoms scattered by the tungsten surface, in the case of an angle of incidence $\beta^i = 45^\circ$. The black and gray symbols correspond to the case of smooth and rough surfaces, respectively. Types of studied surfaces are listed in Table 2. The correlation shown in Fig. 2 can be approximated by the linear function:

$$\langle E^S \rangle = b_B \langle E^i \rangle + b_S (2k_B T_{surf}) \tag{3}$$

where k_B is Boltzhmann's constant, and b_S and b_B are the proportionality factors, which have values of $b_S = 0.18$ and $b_B = 0.77$. The values of b_S and b_B have a 9% difference between similar parameters measured experimentally by Janda et al. [9]. This difference can be explained by the fact that even the best mathematical model is only an approximation of a natural process. Thus, we conclude that achieving a 9% difference is a reasonable result.

An analysis of Eq. (3) allowed us to conclude that if the energy of the incident beam is less than $b_S(2k_B T_{surf})/(1 - b_B)$, then the surface transfers energy to the gas ($E^S > E^i$), otherwise the gas gives energy to the surface ($E^i > E^S$). One can see that data points corresponding to smooth and rough surfaces are very close to each other, which means that the roughness of the surface does not influence the average energy of the scattered gas atoms. However Fig. 3 shows that the ratio (σ_V/μ_V) of root-mean-square deviation (RMSD) to the mean velocity of the atoms scattered by the surface is higher in the case of rough surface when compared to smooth one. If the distribution of random numbers corresponds to a Maxwell–Boltzmann distribution, the relationship between RMSD σ and the mean value μ would be described by the following relation (the following method of analysis based on RMSDs has been proposed in our previous study [17]):

$$\frac{\sigma}{\mu} = \frac{1}{2}\sqrt{\frac{3\pi - 8}{2}} \approx 0.42 \tag{4}$$

The last issue means that the distribution of the velocities of the scattered atoms becomes more Maxwell-like in the case of a rough surface. One can see that the value of σ_V/μ_V more rapidly approaches 0.42 with decreasing incident energy, regardless of the incident polar angle β^i, in the case of an imperfect surface.

Figs. 4 and 5 represent the correlation of the normalized root-mean-square deviation (RMSD) of the azimuthal α^s angle and the polar angle β^s of scattered atoms with energy and angle of incidence. Both polar and azimuthal angles of the scattered atoms were found to vary within the ranges of [−90°; 90°], thus the RMSD corresponding to a uniform distribution for random numbers within this range is:

$$\sigma_{uni} = \frac{b - a}{\sqrt{12}} = \frac{180}{\sqrt{12}} = 30\sqrt{3} \tag{5a}$$

and the normalized RMSDs of scattering of the scattering angles α^s and β^s, can be defined as follows:

$$\tilde{\sigma}_{angle} = \frac{\sigma_{angle}}{\sigma_{uni}} = \frac{\sigma_{angle}}{30\sqrt{3}} \tag{5b}$$

The black symbols in Figs. 4 and 5 correspond to a smooth surface. Based on the results shown in Fig. 4, one could conclude that the mean azimuthal angle of the scattered beam α^s was independent of incident kinetic energy and incident angle β^i when

Table 2
Parameters A and B are the amplitude and wavelength of the roughness on the substrate, respectively.

Surface type	A, 10^{-10} m	B, 10^{-10} m
Type A	0	–
Type B	3.16	6.32
Type C	1.58	6.32
Type D	3.16	12.64
Type E	1.58	12.64

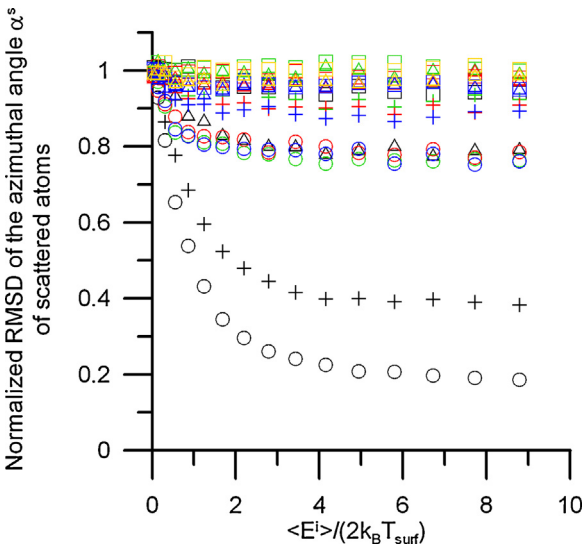

Fig. 4. Normalized root mean square deviation σ_α of the azimuthal angle α^s of scattered atoms versus kinetic energy of impinging atoms and incident polar angle. □, $\beta^i = 10°$; Δ, $\beta^i = 20°$; +, $\beta^i = 40°$; ○, $\beta^i = 60°$. Black symbols correspond to a smooth surface. Green, red, blue and yellow symbols correspond to surfaces of Type B, C, D and E, respectively. (For interpretation of the references to color in this figure legend, the reader is referred to the web version of this article.)

an atom's beam impinged on a rough surface (data points represented by colored symbols). This result is in accordance with results reported by Chase et al. [18]. Fig. 5 presents correlation similar to those shown in Fig. 4, but for the polar angle β^s of the scattered beam. It is clear that the existence of imperfection on the surface reforms the angular distribution of the scattered atoms from normal to almost uniform, i.e., the direction of the velocity vectors of the scattered atoms become independent of the parameters of incidence. Fig. 6a and b represents angular distributions of scattered gas atoms in case of low and high kinetic energy of incidence, respectively. One can see that shape of the density of probability distribution plot of α^s and β^s is insensitive to the surface's roughness in case of low incident energy (see Fig. 6a), while the

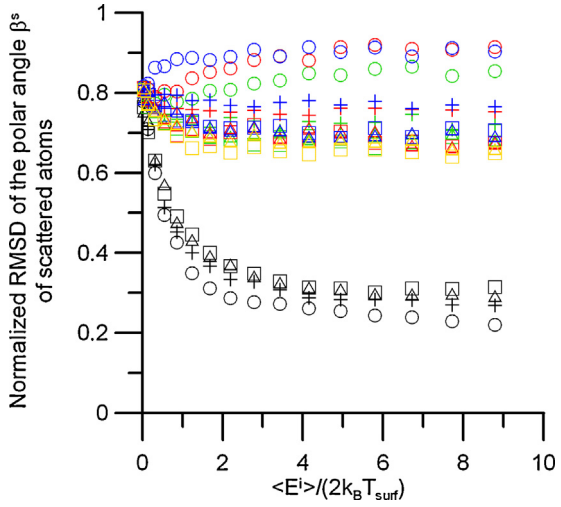

Fig. 5. Normalized root mean square deviation σ_β of the polar angle β^s of scattered atoms versus kinetic energy of impinging atoms and incident polar angle. □, $\beta^i = 10°$; Δ, $\beta^i = 20°$; +, $\beta^i = 40°$; ○, $\beta^i = 60°$. Black symbols correspond to a smooth surface. Green, red, blue and yellow symbols correspond to surfaces of Type B, C, D and E, respectively. (For interpretation of the references to color in this figure legend, the reader is referred to the web version of this article.)

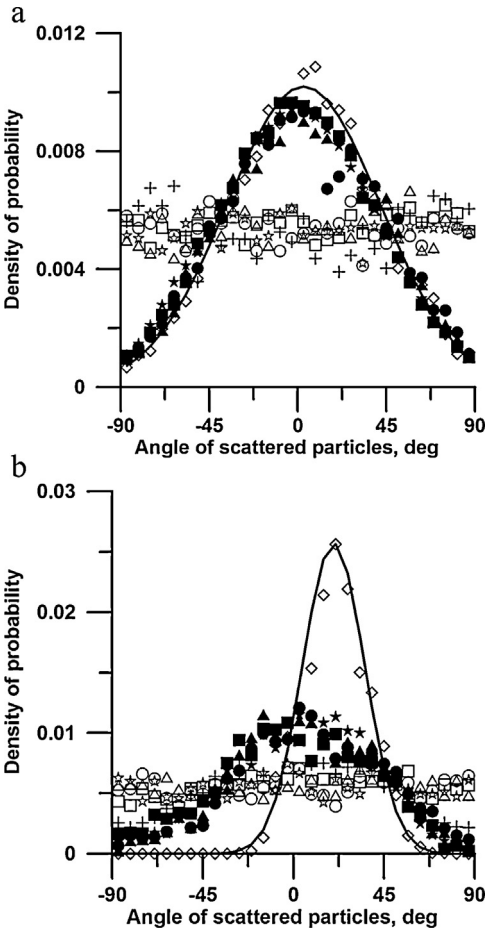

Fig. 6. (a) Density of probability of β^s and α^s. $T_{surf} = 350$ K, $\beta^i = 20°$, $V^i = 100$ m/s. +, Distribution of α^s (surface Type A); ◊, distribution of β^s (surface Type A); solid line – normal distribution of β^s (surface Type A); ○, distribution of α^s (surface Type B); ○, distribution of β^s (surface Type B); Δ, distribution of α^s (surface Type C); ▲, distribution of β^s (surface Type C); □, distribution of α^s (surface Type D); ■, distribution of β^s (surface Type D); ☆, distribution of α^s (surface Type E); ★, distribution of β^s (surface Type E). (b) Density of probability of β^s and α^s. $T_{surf} = 350$ K, $\beta^i = 20°$, $V^i = 1500$ m/s. +, Distribution of α^s (surface Type A); ◊, distribution of β^s (surface Type A); solid line – normal distribution of β^s (surface Type A); ○, distribution of α^s (surface Type B); ○, distribution of β^s (surface Type B); Δ, distribution of α^s (surface Type C); ▲, distribution of β^s (surface Type C); □, distribution of α^s (surface Type D); ■, distribution of β^s (surface Type D); ☆, distribution of α^s (surface Type E); ★, distribution of β^s (surface Type E).

behavior of beam of high incident energy strongly depends on surface's roughness (see Fig. 6b). The last result means that existence even of small imperfection on the surface dramatically changes the consequences of gas-surface interactions.

4. Conclusion

The investigations described above were conducted for various angles of incidents, a series of surface roughness, and varied velocities of impinging Ar atoms (from $V^i = 100$ m/s to 1600 m/s with 100 m/s steps). A total of 400 cases were computed. We have observed that the distribution of the velocities of the scattered atoms becomes more Maxwell-like in the case of a rough surface, while the mean kinetic energy of scattered atoms is almost independent of surface roughness. Furthermore, it was shown that even small surface's irregularities transform gas-surface interactions to more diffusive-like.

Acknowledgments

The authors would like to acknowledge the kind funding support from NSC Taiwan under the contracts of NSC 101-2923-E-006-001-MY3 and NSC 99-2923-E-006-006-MY3.

References

[1] B. Bhushan, Nanotribology and nanomechanics of MEMS/NEMS and BioMEMS/BioNEMS materials and devices, Microelectron. Eng. 84 (3) (2007) 387–412.
[2] T. Fujii, PDMS-based microfluidic devices for biomedical applications, Microelectron. Eng. 61–62 (2002) 907–914.
[3] G.S. Chung, J.M. Jeong, Fabrication of micro heaters on polycrystalline 3C–SiC suspended membranes for gas sensors and their characteristics, Microelectron. Eng. 87 (11) (2010) 2348–2352.
[4] J. Zhou, P. Li, S. Zhang, Y. Huang, P. Yang, M. Bao, G. Ruan, Self-excited piezoelectric microcantilever for gas detection, Microelectron. Eng. 69 (1) (2003) 37–46.
[5] S. Varoutis, D. Valougeorgis, O. Sazhin, F. Sharipov, Rarefied gas flow through short tubes into vacuum, J. Vac. Sci. Technol. A: Vac. Surf. Films 26 (2) (2008) 228–238.
[6] J.C. Maxwell, On stresses in rarified gases arising from inequalities of temperature, Philos. Trans. R. Soc. London, Ser. A 170 (1879) 231–256.
[7] J.K. Roberts, The exchange of energy between gas atoms and solid surfaces, Proc. R. Soc. London, Ser. A 129 (809) (1930) 146–161.
[8] W.H. Weinberg, R.P. Merrill, Scattering of helium, neon, argon, krypton, xenon, and deuterium from a tungsten (1 1 0) surface characterized by LEED, J. Chem. Phys. 56 (6) (1972) 2881–2892.
[9] K.C. Janda, J.E. Hurst, C.A. Becker, J.P. Cowin, D.J. Auerbach, L. Wharton, Direct measurement of velocity distributions in argon beam–tungsten surface scattering, J. Chem. Phys. 72 (4) (1980) 2403–2410.
[10] G. Fan, J.R. Manson, Theory of direct scattering, trapping, and desorption in atom-surface collisions, Phys. Rev. B 79 (4) (2009) 045424.
[11] K.D. Gibson, N. Isa, S.J. Sibener, Experiments and simulations of Ar scattering from an ordered 1-decanethiol–Au(1 1 1) monolayer, J. Chem. Phys. 119 (24) (2003) 13083.
[12] J. Yang, Y. Wang, Y. Chen, GPU accelerated molecular dynamics simulation of thermal conductivities, J. Chem. Phys. 221 (2) (2007) 799–804.
[13] M.S. Friedrichs, P. Eastman, V. Vaidyanathan, M. Houston, S. Legrand, A.L. Beberg, D.L. Ensign, C.M. Bruns, V.S. Pande, Accelerating molecular dynamic simulation on graphics processing units, J. Comput. Chem. 30 (6) (2009) 864–872.
[14] M.S. Ozhgibesov, A.V. Utkin, V.M. Fomin, T.S. Leu, C.H. Cheng, Simulation of copper nanocluster deposition on the contaminated surface using gaming GPU, Int. J. Comput. Mater. Sci. Eng. 01 (01) (2012) 1250007–1250011.
[15] M.S. Ozhgibesov, A.V. Utkin, V.M. Fomin, T.S. Leu, C.H. Cheng, Molecular dynamic simulation of copper nanocluster deposition using graphics processing units (gpu), Comput. Continuum Mech. 5 (2) (2012) 265–273.
[16] G.A. Bird, Molecular Gas Dynamics and the Direct Simulation of Gas Flows, Oxford University Press/Clarendon Press, Oxford/New York, 1994.
[17] T.S. Leu, C.H. Cheng, M.S. Ozhgibesov, New modeling of scattering behaviors of argon atoms on tungsten substrate, J. Mol. Graphics Modell. 31 (0) (2011) 35–40.
[18] D. Chase, M. Manning, J.A. Morgan, G.M. Nathanson, R.B. Gerber, Argon scattering from liquid indium: simulations with embedded atom potentials and experiment, J. Chem. Phys. 113 (20) (2000) 9279–9287.